



Electronic structure based design of thin film metallic glasses with superior fracture toughness

Simon Evertz^{a,*}, Ines Kirchlechner^b, Rafael Soler^b, Christoph Kirchlechner^b, Paraskevas Kontis^b, Jozef Bednarcik^c, Baptiste Gault^{b,d}, Gerhard Dehm^b, Dierk Raabe^b, Jochen M. Schneider^a

^a Materials Chemistry, RWTH Aachen University, Kopernikusstr, 10, 52074 Aachen, Germany

^b Max-Planck-Institut für Eisenforschung, Max-Planck-Str. 1, 40237 Düsseldorf, Germany

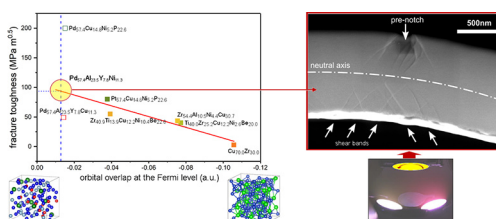
^c Department of Condensed Matter Physics, Institute of Physics, P.J. Safarik University, Park Angelinum 9, 041 54 Kosice, Slovakia

^d Department of Materials, Imperial College, South Kensington, London SW7 2AZ, United Kingdom

HIGHLIGHTS

- A model to quantitatively predict the fracture toughness based on the orbital overlap at the Fermi is introduced.
- The toughness of Pd_{57.4}Al_{23.5}Y_{7.8}Ni_{11.3} metallic glass is predicted to be 95 ± 20 MPa·m^{0.5}
- Pd_{57.4}Al_{23.5}Y_{7.8}Ni_{11.3} metallic glasses show pronounced plasticity and absence of crack growth in micro-mechanical cantilever bending experiments consistent with the predicted toughness.

GRAPHICAL ABSTRACT



ARTICLE INFO

Article history:

Received 19 July 2019

Received in revised form 31 October 2019

Accepted 2 November 2019

Available online 06 November 2019

Keywords:

Metallic glass

Ab initio

Fracture toughness

Chemical bonding

ABSTRACT

High fracture toughness is crucial for the application of metallic glasses as structural materials to avoid catastrophic failure of the material in a brittle manner. One fingerprint for fracture toughness in metallic glasses is the fraction of hybridized bonds, which is affected by alloying Pd_{57.4}Al_{23.5}Y_{7.8}M_{11.3} with M = Fe, Ni, Co, Cu, Os, Ir, Pt, and Au. It is shown that experimental fracture toughness data is correlated to the fraction of hybridized bonds which scale with the localized bonds at the Fermi level. Thus, the localized bonds at the Fermi level are utilized quantitatively as a measure for fracture toughness. Based on *ab initio* calculations, the minimum fraction of hybridized bonds was identified for Pd_{57.4}Al_{23.5}Y_{7.8}Ni_{11.3}. According to the ansatz that the crystal orbital overlap population at the Fermi level scales with fracture toughness, for Pd_{57.4}Al_{23.5}Y_{7.8}Ni_{11.3} a value of around 95 ± 20 MPa·m^{0.5} is predicted quantitatively for the first time. Consistent with this prediction, in micro-mechanical beam bending experiments Pd_{57.4}Al_{23.5}Y_{7.8}Ni_{11.3} thin films show pronounced plasticity and absence of crack growth.

© 2018 The Authors. Published by Elsevier Ltd. This is an open access article under the CC BY license (<http://creativecommons.org/licenses/by/4.0/>).

1. Introduction

Some metallic glasses envisaged for mechanical applications have a high strength [1–3] and show the capability of plastic deformation,

especially in geometries confined to the size of the plastic zone [4,5], which can be in the range of millimeters [6]. Plasticity in metallic glasses is especially reported to occur under bending load [7–10]. Lewandowski et al. put the Poisson's ratio ν forward as a design criterion for brittleness and toughness by reporting a brittle to ductile transition at $\nu = 0.31–0.32$ [11]. However, as this brittle to ductile transition is not universal [9,12,13], Schnabel et al. proposed the fraction of hybridized

* Corresponding author.

E-mail address: evertz@mch.rwth-aachen.de (S. Evertz).

bonds compared to the overall bonding as an electronically motivated measure for high fracture toughness [12] as covalent bonding induces brittleness in metallic glasses [10,14]. Decreasing the fraction of hybridized bonds [12] is therefore proposed to serve as a guideline for increasing fracture toughness. Based on this approach the high fracture toughness of $49.0 \text{ MPa} \cdot \text{m}^{0.5}$ reported for a $\text{Pd}_{57.0}\text{Al}_{23.5}\text{Y}_{7.7}\text{Cu}_{11.4}$ glass can be rationalized by a comparative analysis of densities of states and bonding with brittle metallic glass systems such as $\text{Cu}_{69.6}\text{Zr}_{30.4}$ [12]. For the design of tough metallic glasses, Schnabel's proposal lacks, however, predictive capability since a quantitative relationship between fracture toughness and electronic structure has not been established so far.

Hence, the quantitative model to predict the fracture toughness of metallic glasses based on the fraction of hybridized bonds presented here enables the quantitative prediction of fracture toughness of metallic glasses for the first time. In this model, the crystal orbital overlap population [15] at the Fermi level is utilized as a measure to quantify localized bonds. By correlating the localized bonds with fracture toughness values reported in literature, the fracture toughness of $\text{Pd}_{57.4}\text{Al}_{23.5}\text{Y}_{7.8}\text{Ni}_{11.3}$ is predicted. The prediction from this quantitative model is validated experimentally. Due to its fracture toughness of $49.0 \text{ MPa} \cdot \text{m}^{0.5}$ reported by Schnabel et al. [12], the $\text{Pd}_{57.0}\text{Al}_{23.9}\text{Y}_{7.7}\text{Cu}_{11.4}$ metallic glass is chosen as a reference and $\text{Pd}_{57.0}\text{Al}_{23.9}\text{Y}_{7.7}\text{M}_{11.4}$ ($\text{M} = \text{Fe}, \text{Ni}, \text{Os}, \text{Ir}, \text{Pt}, \text{and Au}$) as the model system with the aim to understand the relationship between electronic structure and fracture toughness by quantification of the fraction of hybridized bonds.

2. Methods

2.1. *Ab initio* calculations

The electronic structure of metallic glasses is the basis for the quantitative model introduced here to predict fracture toughness. To investigate the electronic structure of $\text{Pd}_{57.0}\text{Al}_{23.9}\text{Y}_{7.7}\text{M}_{11.4}$ metallic glasses, *ab initio* molecular dynamics calculations were carried out in this study to determine the fraction of hybridized bonds. Therefore, the density functional theory [16] based openMX code [17,18] was used by employing electronic potentials with the generalized gradient approximation [19]. The following linear combinations of localized pseudoatomic orbitals [20] were applied as basis functions: $\text{Pd}5.0\text{-s}2\text{p}1\text{d}1$, $\text{Al}6.0\text{-s}2\text{p}2$, $\text{Y}6.5\text{-s}3\text{p}2\text{d}1$, $\text{Ni}6.0\text{-s}2\text{p}2\text{d}2\text{f}1$, $\text{Au}8.0\text{-s}2\text{p}2\text{d}1$, $\text{Co}5.5\text{-s}2\text{p}1\text{d}1$, $\text{Ir}7.0\text{-s}2\text{p}2\text{d}2\text{f}1$, $\text{Cu}4.5\text{-s}1\text{p}1\text{d}1$, $\text{Os}7.0\text{-s}2\text{p}2\text{d}2\text{f}1$, $\text{Fe}5.0\text{-s}1\text{p}2\text{d}1$, $\text{Pt}7.0\text{-s}2\text{p}2\text{d}2\text{f}1$. Thereby, the first symbol designates the chemical element followed by the cutoff-radius of the potential in Bohr radii. The last set of symbols defines the primitive orbitals. A grid of $85 \times 85 \times 85$ N-points and a cutoff energy of 150 Ry have been used. The Vienna *Ab initio* Simulation Package (VASP) [21,22] was employed for volume relaxation at 0 K. Therefore, ultrasoft pseudopotentials were employed and the Brillouin zone was integrated at a $3 \times 3 \times 3$ Monkhorst-Pack k -point grid [23]. For the calculation of the electronic structure, projector augmented-wave potentials [22,24] were utilized. The Crystal Orbital Overlap Populations (COOP) [15] and Crystal Hamilton Overlap Populations (COHP) [25] were calculated by the projection of the wavefunction onto localized orbitals using the LOBSTER code (version 2.2.1) [26–28], taking all atomic orbitals in the supercell into account. For visualization, all atomic interactions within the first coordination shell of every atom are considered. To generate glassy structures comparable to experimental samples, the procedure introduced by Hostert et al. [29] was applied. Thereby, a supercell of 115 atoms was heated for 400 fs to 4000 K by scaling the velocities and then quenched to 0 K. Afterwards the volume of the structure was relaxed. The heating-quenching-relaxation cycle was repeated until the volume difference between two subsequent cycles was lower than 2%. To obtain the bulk modulus, the volume-energy data were fitted with the Birch-Murnaghan equation of state [30]. From the atomic positions, the reduced pair distribution function (PDF) $g(r)$ was calculated [29].

2.2. Sample synthesis and characterization

Metallic glass thin films were synthesized by magnetron sputtering from elemental targets on silicon and NaCl-substrates in DC mode in an ultra-high vacuum combinatorial growth system [31] with a base pressure lower than $8 \cdot 10^{-5}$ Pa. The substrate potential was kept floating and no intentional heating was applied. The target to substrate distance was 10 cm. For silicon substrates, no sample rotation was applied to achieve Pd—Ni and Al—Y gradients, from which the position with the calculated composition was selected. For NaCl-substrates, the sample was rotated with 30 rounds per minute to obtain a homogeneous film. The power densities at the targets were 4.2, 4.8, 1.7 and 1.3 W/cm^2 for Pd, Al, Y, and Ni, respectively. Ar was the working gas with a pressure of 0.4 Pa during sputtering [12]. After deposition, the NaCl substrates were dissolved in water, to obtain thin film flakes which were cleaned in isopropanol and acetone prior to the synchrotron measurements. Thin films deposited onto silicon substrates were used for micromechanical testing.

High energy X-ray diffraction (HEXRD) was carried out at beamline P02.1 [32] of the PETRA III electron storage ring at DESY, Hamburg, Germany. X-rays with a wavelength of 0.20701 \AA were utilized. Data were collected with a Perkin Elmer XRD1621 fast detector and processed by applying the FIT2D software [33–35]. The data were corrected for background scattering and the structure factor as well as pair distribution functions calculated by a fast Fourier transformation implemented in the PDFgetX3 software package [36]. The composition of the sample was investigated with an EDAX Genesis 2000 detector on a JEOL JSM-6480 scanning electron microscope. The electronic structure was explored by X-ray photoelectron spectroscopy in a JEOL JAMP 9500F Field Emission Auger microprobe.

The fracture toughness was evaluated using pre-notched micro specimens [37–39] produced *via* focused ion beam (FIB) milling in a Zeiss Auriga® Dual Beam FIB from $1 \mu\text{m}$ thick metallic glass thin films deposited onto Si substrates. Single cantilever bending on pre-notched specimen was used to reduce the possible impact of residual stresses [40]. The ion beam current was sequentially reduced from 2 nA to 50 pA for notching. The nominal dimensions of the cantilever were $1 \times 1 \times 10 \mu\text{m}^3$ with a crack length of 200 nm and a final bending length of $6 \mu\text{m}$ to meet the geometric requirements [41,42] on the used geometry factors. Subsequently, four samples were tested in a Zeiss Gemini 500 field emission scanning electron microscope equipped with an Asmec Unat II *in situ* indenter. The indenter operates in an intrinsic displacement controlled mode [43]. Numerous unloading segments were introduced to the applied displacement function to evaluate crack propagation *via* the unloading stiffness following the small scale approach of Wurster et al. [44]. While small scale fracture tests are not in full geometric accordance with the ASTM K_{IC} measurement standard, reproducible values for fracture toughness are obtained and reported here as K_Q [43].

Atom probe tomography (APT) specimens were prepared from the center of the metallic glass thin film deposited on a silicon substrate using an FEI Helios 600 following procedures described in Ref. [45]. APT measurements were carried out on a Cameca LEAP 3000× HR operated in voltage mode at a pulse repetition rate of 200 kHz, a pulse rate of 15% and the base temperature was set to 60 K. Data analysis was performed using the IVAS 3.8.2 software package.

3. Results and discussion

$\text{Pd}_{57.4}\text{Al}_{23.5}\text{Y}_{7.8}\text{Cu}_{11.3}$ was reported by Schnabel et al. [12] to exhibit a fracture toughness of $49 \text{ MPa} \cdot \text{m}^{0.5}$. Thus, $\text{Pd}_{57.4}\text{Al}_{23.5}\text{Y}_{7.8}\text{Cu}_{11.3}$ was selected as a reference system in the present study. To investigate the composition dependence of the fraction of localized bonds on the overall bonding, Cu in $\text{Pd}_{57.4}\text{Al}_{23.5}\text{Y}_{7.8}\text{Cu}_{11.3}$ has been substituted by Fe, Ni, Co, Os, Ir, Pt, and Au, *i.e.* by screening group 8–11 elements in the 4th and 6th period of the periodic table of elements. In the following, the

results of the *ab initio* calculations are presented. Based on the calculated electronic structure and fracture toughness data from literature, a quantitative model to predict the fracture toughness is introduced. Thereafter, the theoretical atomic scale topology is contrasted to experimental data. Finally, the predicted fracture toughness data and results of micro-mechanical bending tests are compared to critically appraise the prediction.

The total and partial electronic densities of states (DOS) of $\text{Pd}_{57.4}\text{Al}_{23.5}\text{Y}_{7.8}\text{M}_{11.3}$ ($M = \text{Cu, Ir, Au, Ni}$) are presented in Fig. 1 for the energy range of -10 to 0 eV below the Fermi level. The total DOS consist of the sum of the partial DOS of every atom in the supercell of the calculation. The partial DOS contains the summed DOS of all atoms of a certain species. For the partial DOS, the DOS for the s, p and d bands are shown separately to differentiate the individual orbital contributions. The DOS are smoothed by adjacent averaging with a smooth window of 7 data points to enhance clarity. Fig. 1a shows the DOS for the reference material $\text{Pd}_{57.4}\text{Al}_{23.5}\text{Y}_{7.8}\text{Cu}_{11.3}$ [12]. By comparing peak positions and shapes for the main constituents Pd and Al between -5 and -2 eV weak p-d hybridization as well as weak s-d hybridization around -6 eV is observed. While the Y d-band shows only minor overlap with the Pd d-band, strong d-d hybridization between Cu and Pd is present over the complete energy range of -6 to 0 eV populated in the Cu DOS.

Following the approach of Schnabel et al. [12], the hybridizing constituent Cu in the reference $\text{Pd}_{57.4}\text{Al}_{23.5}\text{Y}_{7.8}\text{Cu}_{11.3}$ was substituted in the simulations by Ir, Fe, Os, Pt, Au, Ni to identify a less hybridizing constituent. All compositions discussed here have in common that the main

alloy constituents Pd and Al show weak pd- and sd-hybridization between -6 and -2 eV and that the Y d-band overlaps only slightly with other bands (Fig. 1b–d), as has already been discussed for the reference material above. Therefore, the focus will be on the differences induced by the Cu-substituting element.

The partial DOS of $\text{Pd}_{57.4}\text{Al}_{23.5}\text{Y}_{7.8}\text{Ir}_{11.3}$ (Fig. 1b) resemble those of $\text{Pd}_{57.4}\text{Al}_{23.5}\text{Y}_{7.8}\text{Cu}_{11.3}$. The Ir d-states are more evenly distributed between -6 eV and the Fermi level compared to Cu (Fig. 1a). But as for $\text{Pd}_{57.4}\text{Al}_{23.5}\text{Y}_{7.8}\text{Cu}_{11.3}$, hybridization is evident from the partial DOS of the Ir and Pd d-bands. This type of electronic structure of $\text{Pd}_{57.4}\text{Al}_{23.5}\text{Y}_{7.8}\text{Ir}_{11.3}$ and $\text{Pd}_{57.4}\text{Al}_{23.5}\text{Y}_{7.8}\text{Cu}_{11.3}$ is representative for $\text{Pd}_{57.4}\text{Al}_{23.5}\text{Y}_{7.8}\text{M}_{11.3}$ alloyed with $M = \text{Fe, Os, and Pt}$ (Fig. S1 in the supplementary information).

In contrast to $\text{Pd}_{57.4}\text{Al}_{23.5}\text{Y}_{7.8}\text{Cu}_{11.3}$, the energy range populated by the Au d-band between -6 and -2 eV in $\text{Pd}_{57.4}\text{Al}_{23.5}\text{Y}_{7.8}\text{Au}_{11.3}$ (Fig. 1c) is rather narrow and only weak hybridization with the Pd d-band is found between -6 and -4 eV. In this energy range, however, the total DOS is dominated by the Au d-band. Around -4 eV, sd-hybridization is observed between Al and Au. Due to the small overlap of the Au d-band with the populated states of the other constituents and its domination of the total DOS between -6 and -4 eV, Au should be a suitable candidate element for the substitution of Cu in $\text{Pd}_{57.4}\text{Al}_{23.5}\text{Y}_{7.8}\text{Cu}_{11.3}$ to obtain a metallic glass with high fracture toughness through a low fraction of hybridized bonds.

In the DOS of $\text{Pd}_{57.4}\text{Al}_{23.5}\text{Y}_{7.8}\text{Ni}_{11.3}$ (Fig. 1d), the Ni d-band populates a small energy range between -4 eV and 0 eV similar to

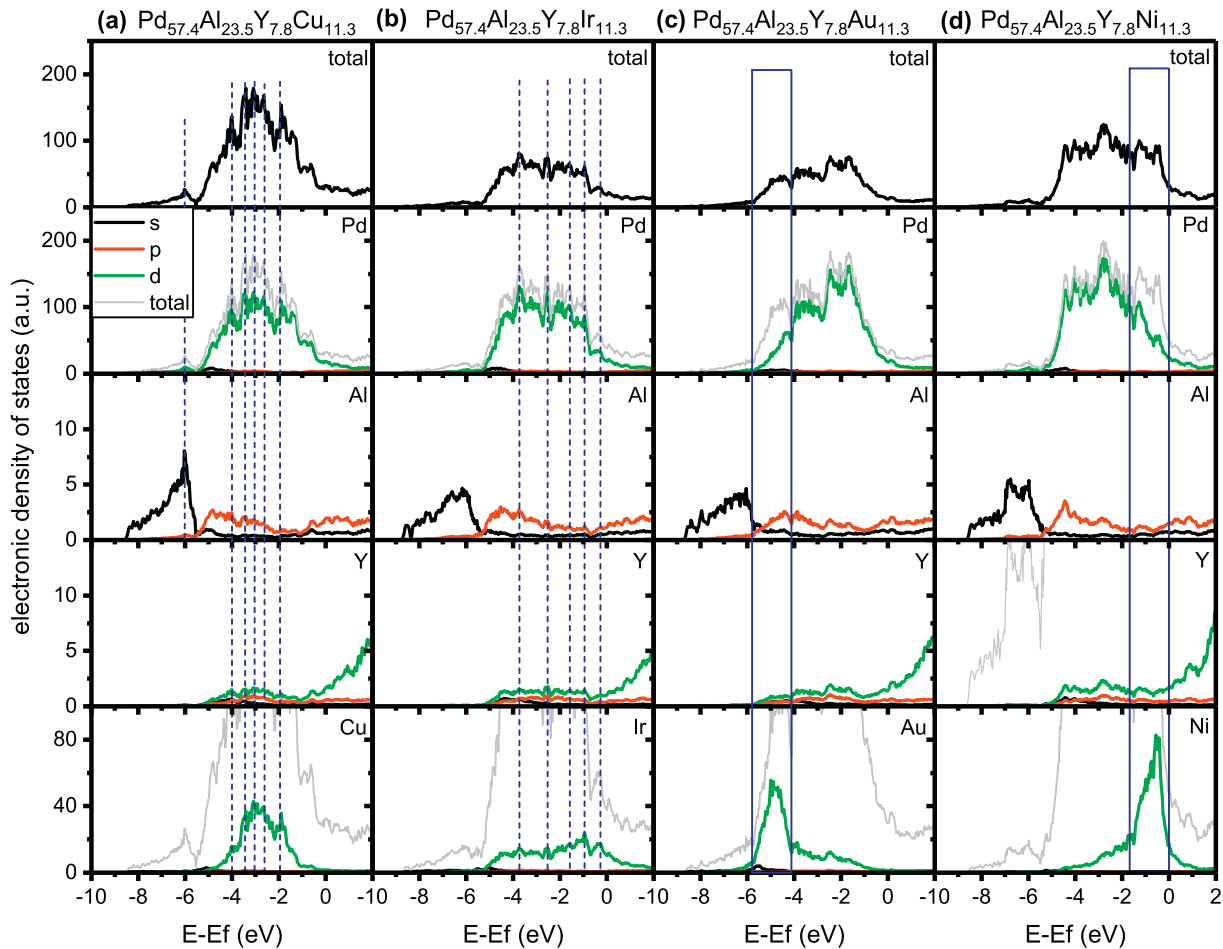


Fig. 1. Total and partial DOS of $\text{Pd}_{57.4}\text{Al}_{23.5}\text{Y}_{7.8}\text{M}_{11.3}$ ($M = \text{Cu, Ir, Au, Ni}$) (a) DOS of reference metallic glass $\text{Pd}_{57.4}\text{Al}_{23.5}\text{Y}_{7.8}\text{Cu}_{11.3}$ and metallic glasses where Cu is replaced by (b) Ir, (c) Au and (d) Ni. The top panels show the total DOS. In the panels of the partial DOS, the states of the s, p and d band are shown with black, red and green lines respectively. The grey line represents the total DOS to relate the partial DOS to the total DOS. In the case of the Ni-containing alloy, the different spin orientations due to spin polarization are summarized. The Fermi-level is shifted to 0 eV. Blue dashed lines indicate hybridization, blue boxes the dominance of the partial DOS of the M elements and are a guide for the eye. (For interpretation of the references to color in this figure legend, the reader is referred to the web version of this article.)

$\text{Pd}_{57.4}\text{Al}_{23.5}\text{Y}_{7.8}\text{Au}_{11.3}$. In this energy range, the Pd d-band becomes less populated, which leads to less hybridization while the Ni d-band dominates the total DOS. In contrast to $\text{Pd}_{57.4}\text{Al}_{23.5}\text{Y}_{7.8}\text{Au}_{11.3}$, due to the vicinity to the Fermi level, the hybridizing states of Ni form weaker bonds compared to the hybridizing states of Au in $\text{Pd}_{57.4}\text{Al}_{23.5}\text{Y}_{7.8}\text{Au}_{11.3}$ that are located at lower energies [15].

Based on the qualitative DOS analysis above, Ni is identified as the most promising candidate to substitute Cu in $\text{Pd}_{57.4}\text{Al}_{23.5}\text{Y}_{7.8}\text{Cu}_{11.3}$ with respect to fracture toughness. While Ir hybridizes strongly with Pd, Au populates only a narrow energy range around -6 eV. However, Ni shows qualitatively the lowest fraction of hybridized bonds on the overall bonding of the transition metals studied here and the hybridizing states of Ni form weak bonds due to the vicinity to the Fermi level [15], thereby promoting shear relaxation.

The bonding and anti-bonding contributions in the Pd-based metallic glass were investigated by the COHP depicted in Fig. 2a. The COHP of $\text{Pd}_{57.4}\text{Al}_{23.5}\text{Y}_{7.8}\text{Ir}_{11.3}$ is smoothed by a Savitzky-Golay [46] filter to enhance the clarity of the graphical representation. According to Rempp [47], these oscillations for $\text{Pd}_{57.4}\text{Al}_{23.5}\text{Y}_{7.8}\text{Ir}_{11.3}$ could

be caused by the energy difference between the Ir d- and both s- and p-bands.

Fig. 2a shows, that the COHPs of the Pd-based metallic glasses from Fig. 1 resemble each other. Below approximately -2.4 eV, the COHPs are negative, indicating bonding contributions to the overall bonding. Above -2.4 eV, all Pd-based metallic glasses show anti-bonding contributions to the bonding. Comparing the COHPs of $\text{Pd}_{57.4}\text{Al}_{23.5}\text{Y}_{7.8}\text{Ir}_{11.3}$ to the reference system $\text{Pd}_{57.4}\text{Al}_{23.5}\text{Y}_{7.8}\text{Cu}_{11.3}$, a slight shift of the COHP above -2.8 eV towards the Fermi level is identified, while it resembles the reference COHP of $\text{Pd}_{57.4}\text{Al}_{23.5}\text{Y}_{7.8}\text{Cu}_{11.3}$ below -2.8 eV. The resulting higher population of anti-bonding states at the Fermi-level indicates weaker bonding. $\text{Pd}_{57.4}\text{Al}_{23.5}\text{Y}_{7.8}\text{Au}_{11.3}$ exhibits fewer bonding contributions than the reference $\text{Pd}_{57.4}\text{Al}_{23.5}\text{Y}_{7.8}\text{Cu}_{11.3}$ between -5 and -3.3 eV, which is part of the energy range dominated by the Au d-band, while its anti-bonding states resemble the reference material. Thus, the lower population of bonding states and the lower fraction of hybridized bonds observed in Fig. 1 results in weaker localized bonds between -5 and -3.3 eV, which may, in turn, enable shear relaxation upon mechanical loading. In contrast to this, the COHP of

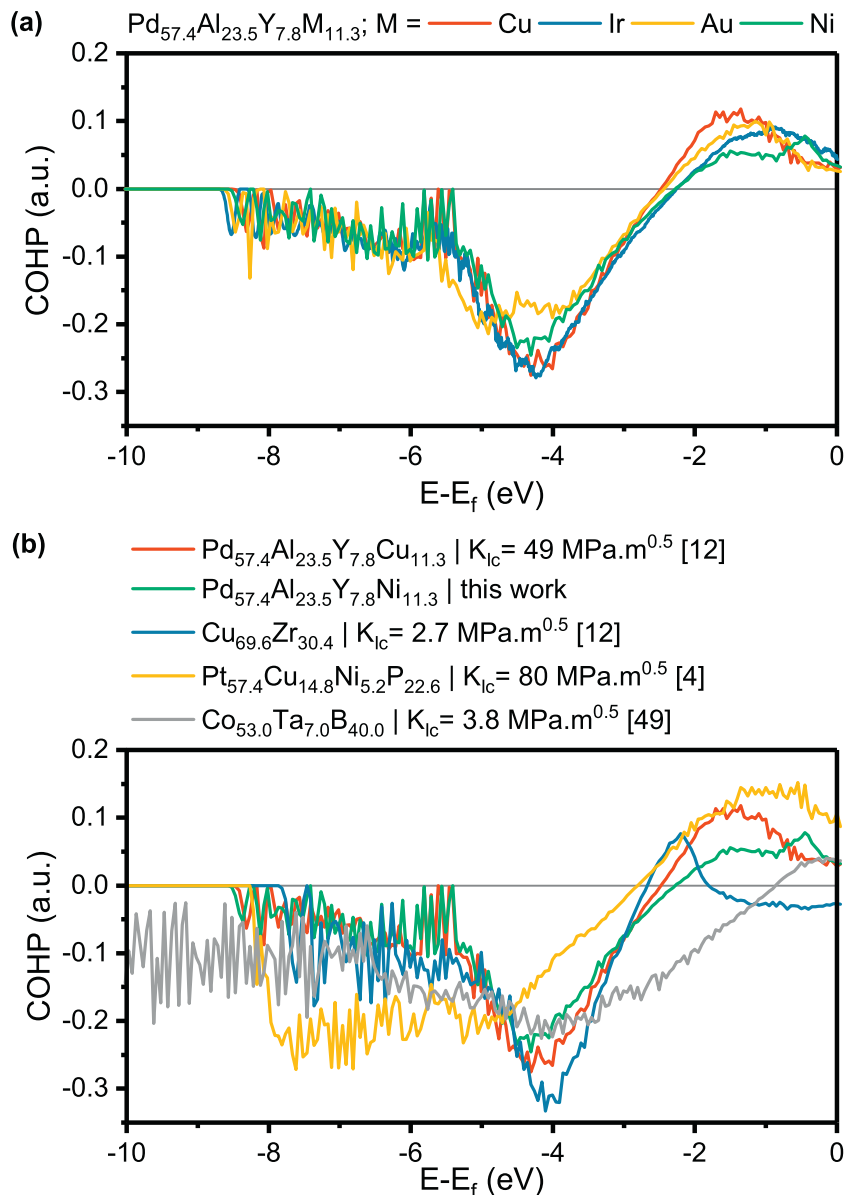


Fig. 2. Crystal Orbital Hamilton Populations (COHP) of (a) $\text{Pd}_{57.4}\text{Al}_{23.5}\text{Y}_{7.8}\text{M}_{11.3}$ ($M = \text{Cu, Ir, Au, Ni}$) metallic glasses shown on Fig. 1 and (b) selected $\text{Pd}_{57.4}\text{Al}_{23.5}\text{Y}_{7.8}\text{M}_{11.3}$ in comparison with $\text{Cu}_{69.6}\text{Zr}_{30.4}$ [12], $\text{Pt}_{57.4}\text{Cu}_{14.8}\text{Ni}_{5.2}\text{P}_{22.6}$ [4] and $\text{Co}_{53.0}\text{Ta}_{7.0}\text{B}_{40.0}$ [49] metallic glasses.

$\text{Pd}_{57.4}\text{Al}_{23.5}\text{Y}_{7.8}\text{Ni}_{11.3}$ resembles the COHP of the reference material in the bonding region, while the anti-bonding contributions are smaller than the reference and shifted to the Fermi-level similar to $\text{Pd}_{57.4}\text{Al}_{23.5}\text{Y}_{7.8}\text{Ir}_{11.3}$. Taking into account the integrated COHP (ICOHP) as a measure of bond strength [48], $\text{Pd}_{57.4}\text{Al}_{23.5}\text{Y}_{7.8}\text{Ni}_{11.3}$ exhibits weaker bonding than $\text{Pd}_{57.4}\text{Al}_{23.5}\text{Y}_{7.8}\text{Au}_{11.3}$ as its ICOHP of -0.509 eV is less negative and hence indicates weaker bond strength than -0.589 eV for $\text{Pd}_{57.4}\text{Al}_{23.5}\text{Y}_{7.8}\text{Au}_{11.3}$, which is consistent with the qualitative DOS analysis above.

Comparing the COHP of $\text{Pd}_{57.4}\text{Al}_{23.5}\text{Y}_{7.8}\text{Cu}_{11.3}$ and $\text{Pd}_{57.4}\text{Al}_{23.5}\text{Y}_{7.8}\text{Ni}_{11.3}$ with the COHP of brittle $\text{Cu}_{69.6}\text{Zr}_{30.4}$ [12], the similarly tough but nearly twice as strong $\text{Co}_{53.0}\text{Ta}_{7.0}\text{B}_{40.0}$ [49] and tough $\text{Pt}_{57.4}\text{Cu}_{14.8}\text{Ni}_{5.2}\text{P}_{22.6}$ [4] shows that $\text{Pd}_{57.4}\text{Al}_{23.5}\text{Y}_{7.8}\text{Ni}_{11.3}$ is similar to the Pt-based metallic glass. Contrary to $\text{Pd}_{57.4}\text{Al}_{23.5}\text{Y}_{7.8}\text{Ni}_{11.3}$, $\text{Pt}_{57.4}\text{Cu}_{14.8}\text{Ni}_{5.2}\text{P}_{22.6}$ exhibits more bonding states between -8 and

-5 eV and at the same time more anti-bonding states close to the Fermi level. Due to the presence of stronger bonding states below -5 eV, $\text{Pt}_{57.4}\text{Cu}_{14.8}\text{Ni}_{5.2}\text{P}_{22.6}$ is expected to be more shear resistant than $\text{Pd}_{57.4}\text{Al}_{23.5}\text{Y}_{7.8}\text{Ni}_{11.3}$. Nevertheless, as the COHP of $\text{Pt}_{57.4}\text{Cu}_{14.8}\text{Ni}_{5.2}\text{P}_{22.6}$ and $\text{Pd}_{57.4}\text{Al}_{23.5}\text{Y}_{7.8}\text{Ni}_{11.3}$ are similar, also the fracture toughness is expected to be similar. The brittle $\text{Cu}_{69.6}\text{Zr}_{30.4}$, in contrast, exhibits anti-bonding states only between -2 and -3 eV and hence bonding states close to the Fermi level, indicating strong, hybridized bonds. The COHP of $\text{Co}_{53.0}\text{Ta}_{7.0}\text{B}_{40.0}$ contains a broad energy range populated by bonding states, anti-bonding states are only present above -1 eV close to the Fermi level. Due to the larger amount of bonding contributions and thus stronger hybridized bonding, the shear resistance in the latter two glasses is predicted to be larger compared to $\text{Pt}_{57.4}\text{Cu}_{14.8}\text{Ni}_{5.2}\text{P}_{22.6}$ and the Pd-based glasses. This prediction is consistent with the brittle behavior reported for $\text{Cu}_{69.6}\text{Zr}_{30.4}$ [12] and

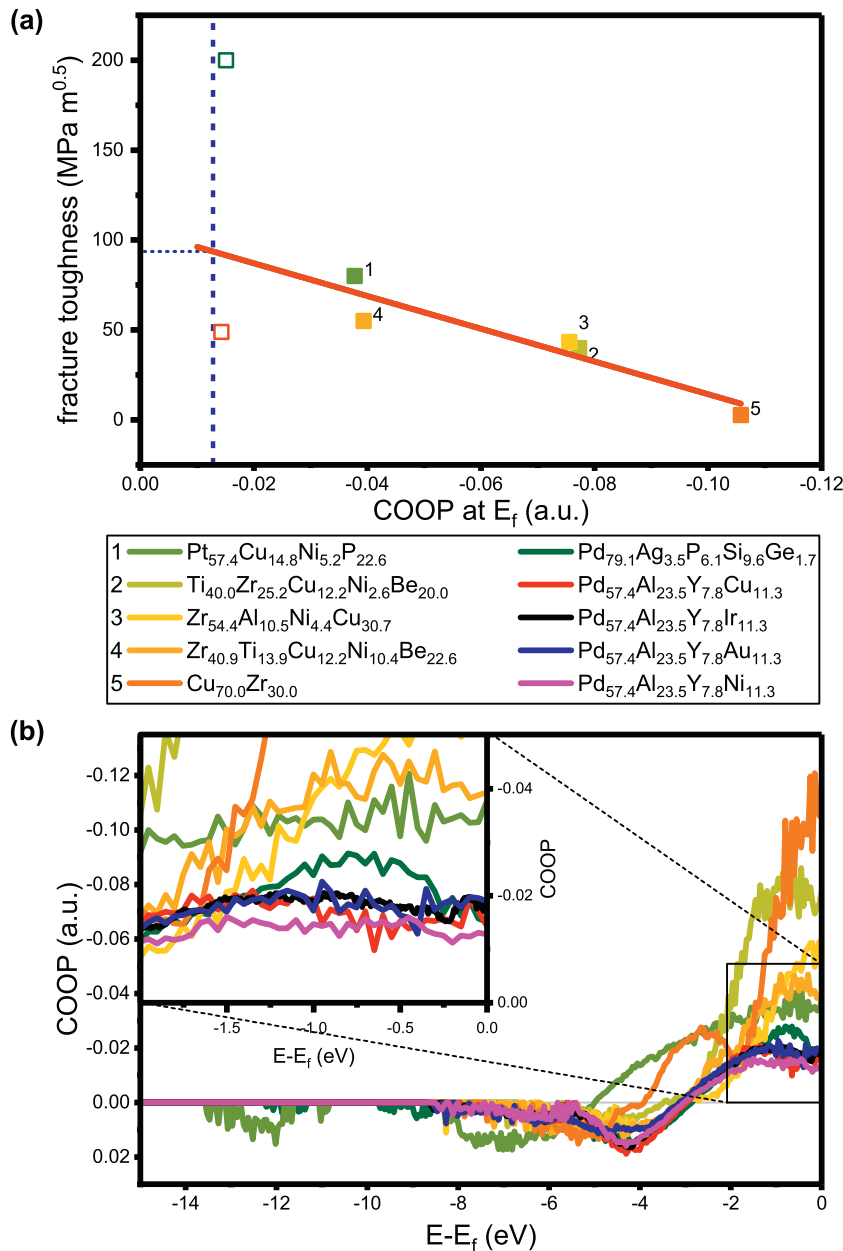


Fig. 3. (a) Fracture toughness as a function of COOP at the Fermi level. Values for fracture toughness were obtained from literature [4,50–54] and COOP calculated by *ab initio* methods. The solid red line represents a linear fit. The blue dashed line marks the COOP at E_f of $\text{Pd}_{57.4}\text{Al}_{23.5}\text{Y}_{7.8}\text{Ni}_{11.3}$. Dotted blue lines mark the minimum and maximum predicted fracture toughness values of $\text{Pd}_{57.4}\text{Al}_{23.5}\text{Y}_{7.8}\text{Ni}_{11.3}$. Note that the fracture toughness of all glasses included in the fit was obtained under similar loading conditions. (b) COOP of metallic glasses from (a) including glasses from Fig. 1. Negative values indicate anti-bonding contributions, positive values bonding contributions. The inset is a magnification of the marked region close to the Fermi level. (For interpretation of the references to color in this figure legend, the reader is referred to the web version of this article.)

$\text{Co}_{53.0}\text{Ta}_{7.0}\text{B}_{40.0}$ [49] in contrast to the plastic behavior reported for $\text{Pt}_{57.4}\text{Cu}_{14.8}\text{Ni}_{5.2}\text{P}_{22.6}$ [4] tested under bending load with slightly different sample sizes [4,12,49].

Above, Ni was identified as the most promising element to substitute Cu in $\text{Pd}_{57.4}\text{Al}_{23.5}\text{Y}_{7.8}\text{Cu}_{11.3}$ to improve fracture toughness. Here, the orbital overlap at the Fermi level is investigated to predict the fracture toughness quantitatively. We assume that for glasses with a low fraction of localized and hence hybridized bonds the balance to the overall bonding is given by metallic bonds. Thus, the ideal glass in terms of toughness exhibits metallic bonds only. By means of Crystal Orbital Overlap Population (COOP) and COHP, it is possible to characterize localized bonding [25], but not metallic bonding directly. Therefore, the fraction of metallic bonding is described indirectly by the absence of localized bonds. Focusing hence on the orbital overlap by means of the COOP, for ideal metallic bonding no localized bond overlap and thus a value of 0 for the COOP at the Fermi level is expected, as all electrons are shared in an electron gas. Due to the pronounced metallic bonding character consistent with the absence of hybridized bonds, a high fracture toughness is expected for metallic glasses with a low COOP at the Fermi level.

The fracture toughness of non-magnetic metallic glasses reported in literature [4,50–54] is presented in Fig. 3a) as a function of the COOP at the Fermi level. Therefore, we use the same data set for fracture toughness as Demetriou et al. [50] expanded by the data from Schnabel et al. [12]. These data are fitted by a linear fit excluding fracture toughness values of $\text{Pd}_{79.1}\text{Ag}_{3.5}\text{P}_{6.1}\text{Si}_{9.6}\text{Ge}_{1.7}$ and $\text{Pd}_{57.4}\text{Al}_{23.5}\text{Y}_{7.8}\text{Cu}_{11.3}$, as these data may be affected by sample size: The fracture toughness of $\text{Pd}_{79.1}\text{Ag}_{3.5}\text{P}_{6.1}\text{Si}_{9.6}\text{Ge}_{1.7}$ might be overestimated because the plastic zone size of 6 mm is larger than the actual sample size [50] of $2.1 \times 2.1 \times 20 \text{ mm}^3$ in two dimensions [5]. Fracture toughness of $\text{Pd}_{57.4}\text{Al}_{23.5}\text{Y}_{7.8}\text{Cu}_{11.3}$ is determined by the J-integral and might be sample size dependent [12]. The COOP at the Fermi level of $\text{Pd}_{57.4}\text{Al}_{23.5}\text{Y}_{7.8}\text{Ni}_{11.3}$ is indicated by a dashed blue line. Based on the intersection of the dashed blue line with the fit, the fracture toughness of $\text{Pd}_{57.4}\text{Al}_{23.5}\text{Y}_{7.8}\text{Ni}_{11.3}$ is predicted to be around $95 \pm 20 \text{ MPa} \cdot \text{m}^{0.5}$. Comparing this prediction with the Ashby map reported by Demetriou et al. [50], this predicted fracture toughness corresponds to a plastic zone size in the orders of 0.1 to 1 mm [50]. Furthermore, this analysis shows that in addition to the presence of localized bonds, also anti-bonding states at the Fermi level must be considered for the design of tough metallic glasses. Antibonding states increase the total bond energy and thus promote bond separation [55] and hence favor brittle behavior of metallic glasses. Due to the promotion of bond separation, not only the fracture toughness is affected by anti-bonding states, but also the cohesive energy and hence the elastic properties (cf. Fig. S2). The free volume in *ab initio* calculations is small and different free volume configurations were not tested. Hence, the free volume content is smaller than it might be in physical samples, as shown in Fig. 4 below. However, as a larger amount of free volume promotes fracture toughness by lowering the energy barrier for shear transformation and plastic deformation [56], the fracture toughness predicted based on the electronic structure serves as a lower bound while free volume affects the variability of fracture toughness observed in Fig. 3a.

The COOP of the glasses presented in Figs. 1 and 3a) are shown in Fig. 3b). While all material systems exhibit a transition between bonding and anti-bonding states between -5 and -3 eV, the amount of anti-bonding states close to the Fermi level differs significantly. It is evident that the difference between the COOPs depends mainly on the major constituent of the alloys. The difference between the Pd-based metallic glasses is hence rather small (inset Fig. 3b). Nevertheless, $\text{Pd}_{57.4}\text{Al}_{23.5}\text{Y}_{7.8}\text{Ni}_{11.3}$ clearly exhibits the smallest population of anti-bonding states at the Fermi level ($\text{COOP}(E_f)_{\text{Ni}} = -0.01278$), whereas $\text{Pd}_{57.4}\text{Al}_{23.5}\text{Y}_{7.8}\text{Au}_{11.3}$ – from a qualitative point of view (Fig. 1) also interesting – displays a larger population of anti-bonding states at the Fermi level ($\text{COOP}(E_f)_{\text{Au}} = -0.01901$). Therefore, the predicted fracture toughness of approximately $95 \pm 20 \text{ MPa} \cdot \text{m}^{0.5}$ of

$\text{Pd}_{57.4}\text{Al}_{23.5}\text{Y}_{7.8}\text{Ni}_{11.3}$ is the largest within the here considered group of metallic glasses.

Since the Ni-containing Pd-based metallic glass is the most promising candidate in terms of fracture toughness, this composition was synthesized by magnetron sputtering in the form of a $\text{Pd}_{57.9}\text{Al}_{25.0}\text{Y}_{4.9}\text{Ni}_{12.2}$ thin film on silicon and $\text{Pd}_{62.1}\text{Al}_{27.3}\text{Y}_{4.2}\text{Ni}_{6.4}$ for the thin film flakes. The constituents are homogeneously distributed based on the frequency distribution analysis performed on data collected by atom probe tomography (see Fig. S3 in supplementary information). Hence, chemical inhomogeneities on the here probed length scale cannot be revealed by atom probe tomography. To critically appraise the predicted topology, the calculated pair distribution function is compared to the experimentally obtained one in Fig. 4a. Considering the slight differences between the composition of the powder and the calculation, the pair distribution functions are in reasonable agreement. However, the first peak of the experimental pair distribution function is shifted to a larger bond distance compared to the theoretical one. This indicates that the synthesized material is less frustrated, most likely due to the presence of free volume. As the energy barrier for shear transformation and thus plastic deformation, which is required for high fracture toughness, decreases with increasing free volume content in the sample [56], the plastic deformation behavior of the experimental sample is expected to be more enhanced than predicted with the fracture toughness predicted serving as a lower bound. Fig. 4b compares the theoretical DOS with the experimental DOS. Due to the high energy of the X-rays in the XPS (1.49 keV) as well as the temperature in the experiment (298 K in experiment vs. 0 K in the calculation), the experimental DOS experiences severe peak broadening. Thereby, one broad hump is observed for the valence band, that covers the energy range of the more detailed theoretical DOS. The comparison between calculated and measured topology and electronic structure confirms the significance of the *ab initio* modeled structure.

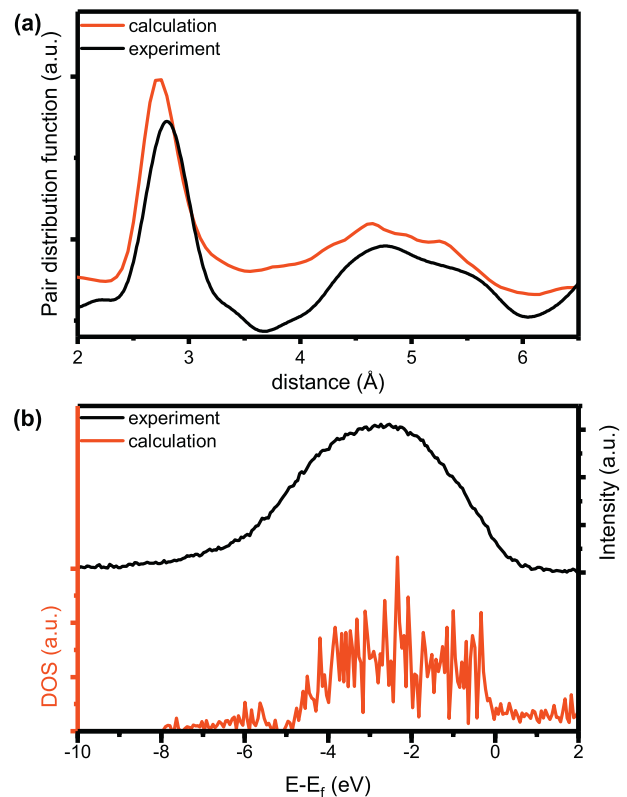


Fig. 4. (a) Calculated and experimental pair distribution function of $\text{Pd}_{57.4}\text{Al}_{23.5}\text{Y}_{7.8}\text{Ni}_{11.3}$ and $\text{Pd}_{62.1}\text{Al}_{27.3}\text{Y}_{4.2}\text{Ni}_{6.4}$, respectively. The experimental PDF has already been published in [57]. (b) Calculated density of states of $\text{Pd}_{57.4}\text{Al}_{23.5}\text{Y}_{7.8}\text{Ni}_{11.3}$ and the valence band of $\text{Pd}_{62.1}\text{Al}_{27.3}\text{Y}_{4.2}\text{Ni}_{6.4}$ measured by XPS.

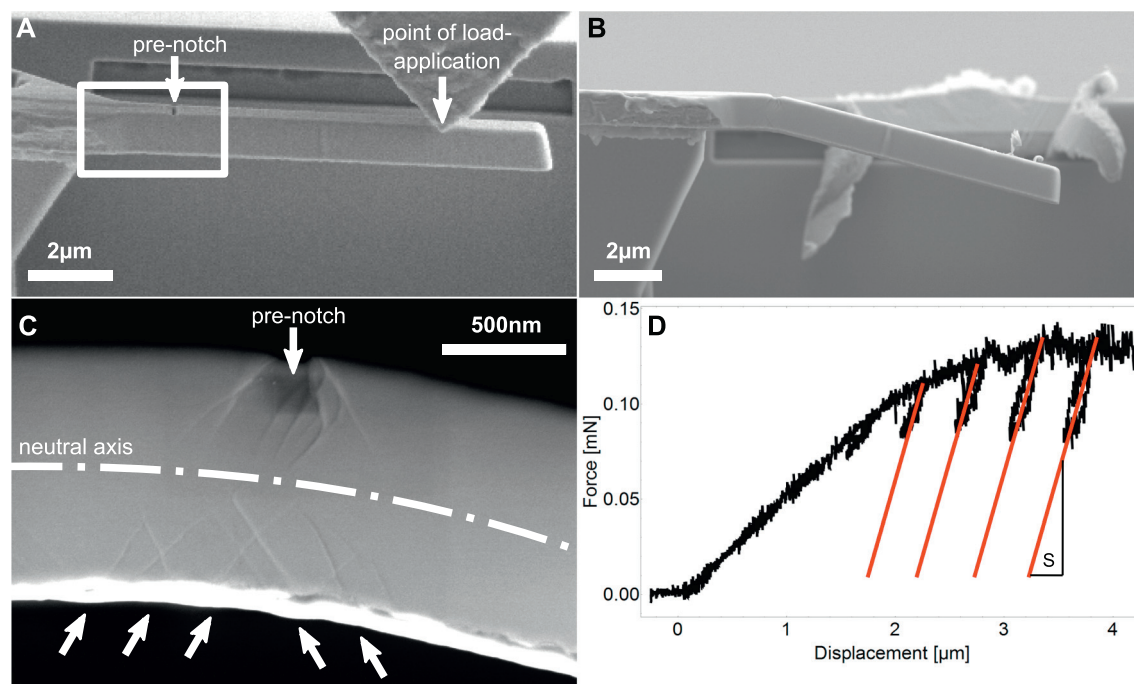


Fig. 5. (a) Snapshot of $\text{Pd}_{57.9}\text{Al}_{25.0}\text{Y}_{4.9}\text{Ni}_{12.2}$ micro cantilever during *in situ* loading. (b) *Post mortem* microbeam after $4\ \mu\text{m}$ deflection. (c) Detail in-lense-SE micrograph of the region highlighted in (a). Huge shear bands are formed at the location of the pre-notch. The arrows indicate the additional formation of shear bands at the compression side of the cantilever. (d) Force versus displacement raw-data. The unloading stiffness (S in Fig. 5d) shown in red does not significantly change during the experiment indicating an absence of substantial crack-growth. Plasticity in the vicinity of the pre-notch is observed right from the beginning resulting in a different initial loading slope compared to S . (For interpretation of the references to color in this figure legend, the reader is referred to the web version of this article.)

To investigate the fracture toughness of the $\text{Pd}_{57.9}\text{Al}_{25.0}\text{Y}_{4.9}\text{Ni}_{12.2}$ metallic glass, beams were prepared for micro-mechanical testing (Fig. 5a). The unloading slopes (S in Fig. 5d) performed after 2, 2.5, 3, and $3.5\ \mu\text{m}$ displacement do not change indicating an absence of crack extension. Also, at the final displacement of $4\ \mu\text{m}$, the beam did not fracture (Fig. 5b). In contrast, multiple shear-bands are formed not only around the pre-notch but also on the compressive side of the cantilever (Fig. 5c) indicating significant plastic deformation. The shear bands do not cross the neutral axis which indicates that shear band propagation is suppressed by the stress gradient and the change from tensile to compressive stresses across cantilever. Therefore, catastrophic shear band propagation is prevented because the suppressed shear band propagation requires the activation of new shear bands (see Fig. 5c) and allows the glass to deform plastically without catastrophic crack development [5] up to the final displacement of $4\ \mu\text{m}$. Since no evidence for crack extension was obtained in *post mortem* imaging, the fracture toughness exceeds the constraints of micromechanical fracture experiments. This is in agreement with the high fracture toughness expected from the plot in Fig. 3, which would require substantially larger samples to quantitatively prove the enormous fracture toughness [5,58]. Such sample dimensions are – in light of the chemical composition and technological constraints – currently not feasible.

4. Conclusions

Inspired by the qualitative notion of Schnabel et al. [12] that the fraction of bonds stemming from hybridized states compared to the overall bonding can be associated with damage tolerance in thin film metallic glasses, a correlation between the fraction of localized and anti-bonding bonds scaling with the crystal orbital overlap population at the Fermi level and experimental fracture toughness data is identified. It is shown that a low number of anti-bonding states at the Fermi-level is a necessary requirement for high fracture toughness. The electronic structures of $\text{Pd}_{57.4}\text{Al}_{23.5}\text{Y}_{7.8}\text{M}_{11.3}$ ($M = \text{Fe, Ni, Cu, Os, Ir, Pt, and Au}$) have been calculated by *ab initio* methods. $\text{Pd}_{57.4}\text{Al}_{23.5}\text{Y}_{7.8}\text{Ni}_{11.3}$ was identified to exhibit

the minimal fraction of hybridized bonds of the materials investigated. Moreover, the correlation between the fraction of localized anti-bonding bonds scaling with the crystal orbital overlap population at the Fermi level and experimental fracture toughness data was identified. This correlation allows the quantitative prediction of fracture toughness of metallic glasses that is crucial for the design of tough metallic glasses. With this model, the fracture toughness of $\text{Pd}_{57.4}\text{Al}_{23.5}\text{Y}_{7.8}\text{Ni}_{11.3}$ is predicted to be $95 \pm 20\ \text{MPa}\cdot\text{m}^{0.5}$, being the first fracture toughness value predicted quantitatively for a metallic glass based on the electronic structure. Consistent with this prediction, micro-mechanical beam bending experiments show that $\text{Pd}_{57.4}\text{Al}_{23.5}\text{Y}_{7.8}\text{Ni}_{11.3}$ thin films exhibit superior fracture toughness and form multiple shear bands.

CRediT authorship contribution statement

Simon Evertz: Conceptualization, Methodology, Formal analysis, Investigation, Writing - Original Draft. **Ines Kirchlechner:** Conceptualization, Methodology, Formal analysis, Investigation, Writing - Original Draft. **Rafael Soler:** Conceptualization, Methodology, Formal analysis, Investigation, Writing - Original Draft. **Christoph Kirchlechner:** Conceptualization, Methodology, Formal analysis, Investigation, Writing - Original Draft. **Paraskevas Kontis:** Conceptualization, Methodology, Formal analysis, Investigation, Writing - Original Draft. **Jozef Bednarcik:** Methodology, Formal analysis, Investigation, Writing - Original Draft. **Baptiste Gault:** Conceptualization, Methodology, Formal analysis, Writing - Original Draft. **Gerhard Dehm:** Conceptualization, Writing - Original Draft, Supervision, Funding acquisition. **Dierk Raabe:** Conceptualization, Writing - Original Draft, Supervision, Funding acquisition. **Jochen M. Schneider:** Conceptualization, Writing - Original Draft, Supervision, Funding acquisition.

Acknowledgements

We thank D. Music for fruitful discussions about the *ab initio* calculations. Financial support of the German Research Foundation within the

SPP 1594 “Topological engineering of Ultrastrong Glasses” is acknowledged (DE 796/9-2, SCHN 735/22-2, RA 123). *Ab initio* calculations were performed on the JARA-HPC Partition part of the supercomputer CLAIK at RWTH Aachen University within the project JARA0131. Parts of this research were carried out at beamline PO2.1 of the light source PETRA III at DESY, a member of the Helmholtz Association (HGF).

Data availability

The raw/processed data required to reproduce these findings cannot be shared at this time due to technical or time limitations.

Declaration of competing interest

None.

Appendix A. Supplementary data

Supplementary data to this article can be found online at <https://doi.org/10.1016/j.matdes.2019.108327>.

References

- [1] M. Telford, The case for bulk metallic glass, *Mater. Today* 7 (2004) 36–43, [https://doi.org/10.1016/S1369-7021\(04\)00124-5](https://doi.org/10.1016/S1369-7021(04)00124-5).
- [2] M. Ashby, A.L. Greer, Metallic glasses as structural materials, *Scr. Mater.* 54 (2006) 321–326, <https://doi.org/10.1016/j.scriptamat.2005.09.051>.
- [3] A. Inoue, B. Shen, A. Takeuchi, Developments and applications of bulk glassy alloys in late transition metal base system, *Mater. Trans.* 47 (2006) 1275–1285, <https://doi.org/10.2320/matertrans.47.1275>.
- [4] J. Schroers, W.L. Johnson, Ductile bulk metallic glass, *Phys. Rev. Lett.* 93 (2004), 255506, <https://doi.org/10.1103/PhysRevLett.93.255506>.
- [5] B. Gludovatz, D. Granata, K.V.S. Thurston, J.F. Löffler, R.O. Ritchie, On the understanding of the effects of sample size on the variability in fracture toughness of bulk metallic glasses, *Acta Mater.* 126 (2017) 494–506, <https://doi.org/10.1016/j.actamat.2016.12.054>.
- [6] J. Schroers, Processing of bulk metallic glass, *Adv. Mater.* 22 (2010) 1566–1597, <https://doi.org/10.1002/adma.200902776>.
- [7] X.K. Xi, D.Q. Zhao, M.X. Pan, W.H. Wang, Y. Wu, J.J. Lewandowski, Fracture of brittle metallic glasses: brittleness or plasticity, *Phys. Rev. Lett.* 94 (2005), 125510, <https://doi.org/10.1103/PhysRevLett.94.125510>.
- [8] W. Chen, J. Ketkaew, Z. Liu, R.M.O. Mota, K. O'Brien, C.S. da Silva, et al., Does the fracture toughness of bulk metallic glasses scatter? *Scr. Mater.* 107 (2015) 1–4, <https://doi.org/10.1016/j.scriptamat.2015.05.003>.
- [9] Z.-d. Zhu, P. Jia, J. Xu, Optimization for toughness in metalloid-free Ni-based bulk metallic glasses, *Scr. Mater.* 64 (2011) 785–788, <https://doi.org/10.1016/j.scriptamat.2010.12.047>.
- [10] Q. He, Y.-Q. Cheng, E. Ma, J. Xu, Locating bulk metallic glasses with high fracture toughness: chemical effects and composition optimization, *Acta Mater.* 59 (2011) 202–215, <https://doi.org/10.1016/j.actamat.2010.09.025>.
- [11] J.J. Lewandowski, W.H. Wang, A.L. Greer, Intrinsic plasticity or brittleness of metallic glasses, *Philos. Mag. Lett.* 85 (2005) 77–87, <https://doi.org/10.1080/09500830500080474>.
- [12] V. Schnabel, B.N. Jaya, M. Köhler, D. Music, C. Kirchlechner, G. Dehm, et al., Electronic hybridisation implications for the damage-tolerance of thin film metallic glasses, *Sci. Rep.* 6 (2016), 36556, <https://doi.org/10.1038/srep36556>.
- [13] R. Raghavan, P. Murali, U. Ramamurty, On factors influencing the ductile-to-brittle transition in a bulk metallic glass, *Acta Mater.* 57 (2009) 3332–3340, <https://doi.org/10.1016/j.actamat.2009.03.047>.
- [14] T. Rouxel, Fracture surface energy and toughness of inorganic glasses, *Scr. Mater.* 137 (2017) 109–113, <https://doi.org/10.1016/j.scriptamat.2017.05.005>.
- [15] R. Hoffmann, How chemistry and physics meet in the solid state, *Angew. Chem. Int. Ed. Eng.* 26 (1987) 846–878, <https://doi.org/10.1002/anie.198708461>.
- [16] P. Hohenberg, W. Kohn, Inhomogeneous electron gas, *Phys. Rev.* 136 (1964) B864–B871, <https://doi.org/10.1103/PhysRev.136.B864>.
- [17] T. Ozaki, H. Kino, Numerical atomic basis orbitals from H to Kr, *Phys. Rev. B* 69 (2004), 195113, <https://doi.org/10.1103/PhysRevB.69.195113>.
- [18] T. Ozaki, H. Kino, Efficient projector expansion for the *ab initio* LCAO method, *Phys. Rev. B* 72 (2005), 045121, <https://doi.org/10.1103/PhysRevB.72.045121>.
- [19] J.P. Perdew, K. Burke, M. Ernzerhof, Generalized gradient approximation made simple, *Phys. Rev. Lett.* 77 (1996) 3865–3868, <https://doi.org/10.1103/PhysRevLett.77.3865>.
- [20] T. Ozaki, Variationally optimized atomic orbitals for large-scale electronic structures, *Phys. Rev. B* 67 (2003), 155108, <https://doi.org/10.1103/PhysRevB.67.155108>.
- [21] G. Kresse, J. Furthmüller, Efficient iterative schemes for *ab initio* total-energy calculations using a plane-wave basis set, *Phys. Rev. B* 54 (1996) 11169–11186, <https://doi.org/10.1103/PhysRevB.54.11169>.
- [22] G. Kresse, D. Joubert, From ultrasoft pseudopotentials to the projector augmented-wave method, *Phys. Rev. B* 59 (1999) 1758–1775, <https://doi.org/10.1103/PhysRevB.59.1758>.
- [23] H.J. Monkhorst, J.D. Pack, Special points for Brillouin-zone integrations, *Phys. Rev. B* 13 (1976) 5188–5192, <https://doi.org/10.1103/PhysRevB.13.5188>.
- [24] P.E. Blöchl, Projector augmented-wave method, *Phys. Rev. B* 50 (1994) 17953–17979, <https://doi.org/10.1103/PhysRevB.50.17953>.
- [25] R. Dronskowski, P.E. Blöchl, Crystal orbital Hamilton populations (COHP): energy-resolved visualization of chemical bonding in solids based on density-functional calculations, *J. Phys. Chem.* 97 (1993) 8617–8624, <https://doi.org/10.1021/j100135a014>.
- [26] V.L. Deringer, A.L. Tchougréeff, R. Dronskowski, Crystal orbital Hamilton population (COHP) analysis as projected from plane-wave basis sets, *J. Phys. Chem. A* 115 (2011) 5461–5466, <https://doi.org/10.1021/jp202489s>.
- [27] S. Maintz, V.L. Deringer, A.L. Tchougréeff, R. Dronskowski, Analytic projection from plane-wave and PAW wavefunctions and application to chemical-bonding analysis in solids, *J. Comput. Chem.* 34 (2013) 2557–2567, <https://doi.org/10.1002/jcc.23424>.
- [28] S. Maintz, V.L. Deringer, A.L. Tchougréeff, R. Dronskowski, LOBSTER: a tool to extract chemical bonding from plane-wave based DFT, *J. Comput. Chem.* 37 (2016) 1030–1035, <https://doi.org/10.1002/jcc.24300>.
- [29] C. Hostert, D. Music, J. Bednarcik, J. Keckes, V. Kapaklis, B. Hjörvarsson, et al., *Ab initio* molecular dynamics model for density, elastic properties and short range order of Co-Fe-Ta-B metallic glass thin films, *J. Phys. Condens. Matter* 23 (2011), 475401, <https://doi.org/10.1088/0953-8984/23/47/475401>.
- [30] F. Birch, Finite strain isotherm and velocities for single-crystal and polycrystalline NaCl at high pressures and 300°K, *J. Geophys. Res.* 83 (1978) 1257, <https://doi.org/10.1029/JB083iB03p01257>.
- [31] V. Schnabel, M. Köhler, S. Evertz, J. Gamcova, J. Bednarcik, D. Music, et al., Revealing the relationships between chemistry, topology and stiffness of ultrastrong Co-based metallic glass thin films: a combinatorial approach, *Acta Mater.* 107 (2016) 213–219, <https://doi.org/10.1016/j.actamat.2016.01.060>.
- [32] A.-C. Dippel, H.-P. Liemann, J.T. Delitz, P. Walter, H. Schulte-Schrepping, O.H. Seeck, et al., Beamline PO2.1 at PETRA III for high-resolution and high-energy powder diffraction, *J. Synchrotron Radiat.* 22 (2015) 675–687, <https://doi.org/10.1107/S1600577515002222>.
- [33] A.P. Hammersley, *FT2D: An Introduction and Overview*, ESRF, Grenoble, 1997.
- [34] A.P. Hammersley, S.O. Svensson, A. Thompson, Calibration and correction of spatial distortions in 2D detector systems, *Nucl. Instrum. Meth. A* 346 (1994) 312–321, [https://doi.org/10.1016/0168-9002\(94\)90720-X](https://doi.org/10.1016/0168-9002(94)90720-X).
- [35] A.P. Hammersley, S.O. Svensson, M. Hanfland, A.N. Fitch, D. Hausermann, Two-dimensional detector software: from real detector to idealised image or two-theta scan, *High Pressure Res.* 14 (1996) 235–248, <https://doi.org/10.1080/08957959608201408>.
- [36] P. Juhás, T. Davis, C.L. Farrow, S.J.L. Billinge, PDFgetX3: a rapid and highly automatable program for processing powder diffraction data into total scattering pair distribution functions, *J. Appl. Crystallogr.* 46 (2013) 560–566, <https://doi.org/10.1107/S0021889813005190>.
- [37] K. Matoy, H. Schönherr, T. Detzel, T. Schöberl, R. Pippan, C. Motz, et al., A comparative micro-cantilever study of the mechanical behavior of silicon based passivation films, *Thin Solid Films* 518 (2009) 247–256, <https://doi.org/10.1016/j.tsf.2009.07.143>.
- [38] D. Di Maio, S.G. Roberts, Measuring fracture toughness of coatings using focused-ion-beam-machined microbeams, *J. Mater. Res.* 20 (2005) 299–302, <https://doi.org/10.1557/JMR.2005.0048>.
- [39] R. Pippan, S. Wurster, D. Kiener, Fracture mechanics of micro samples: fundamental considerations, *Mater. Des.* 159 (2018) 252–267, <https://doi.org/10.1016/j.matdes.2018.09.004>.
- [40] B.N. Jaya, C. Kirchlechner, G. Dehm, Can microscale fracture tests provide reliable fracture toughness values?: a case study in silicon, *J. Mater. Res.* 30 (2015) 686–698, <https://doi.org/10.1557/jmr.2015.2>.
- [41] S. Brinckmann, C. Kirchlechner, G. Dehm, Stress intensity factor dependence on anisotropy and geometry during micro-fracture experiments, *Scr. Mater.* 127 (2017) 76–78, <https://doi.org/10.1016/j.scriptamat.2016.08.027>.
- [42] S. Brinckmann, K. Matoy, C. Kirchlechner, G. Dehm, On the influence of microcantilever pre-crack geometries on the apparent fracture toughness of brittle materials, *Acta Mater.* 136 (2017) 281–287, <https://doi.org/10.1016/j.actamat.2017.07.014>.
- [43] G. Dehm, B.N. Jaya, R. Raghavan, C. Kirchlechner, Overview on micro- and nanomechanical testing: new insights in interface plasticity and fracture at small length scales, *Acta Mater.* 142 (2018) 248–282, <https://doi.org/10.1016/j.actamat.2017.06.019>.
- [44] S. Wurster, C. Motz, R. Pippan, Characterization of the fracture toughness of micro-sized tungsten single crystal notched specimens, *Philos. Mag.* 92 (2012) 1803–1825, <https://doi.org/10.1080/14786435.2012.658449>.
- [45] K. Thompson, D. Lawrence, D.J. Larson, J.D. Olson, T.F. Kelly, B. Gorman, In situ site-specific specimen preparation for atom probe tomography, *Ultramicroscopy* 107 (2007) 131–139, <https://doi.org/10.1016/j.ultramicro.2006.06.008>.
- [46] A. Savitzky, M.J.E. Golay, Smoothing and differentiation of data by simplified least squares procedures, *Anal. Chem.* 36 (1964) 1627–1639, <https://doi.org/10.1021/ac60214a047>.
- [47] H. Rempp, On the electronic density of states of the transition metals, *Z. Physik* 267 (1974) 181–186, <https://doi.org/10.1007/BF01669218>.
- [48] V.L. Deringer, W. Zhang, M. Lumeij, S. Maintz, M. Wuttig, R. Mazzarello, et al., Bonding nature of local structural motifs in amorphous GeTe, *Angew. Chem. Int. Ed. Eng.* 53 (2014) 10817–10820, <https://doi.org/10.1002/anie.201404223>.
- [49] P. Kontis, M. Köhler, S. Evertz, Y.-T. Chen, V. Schnabel, R. Soler, et al., Nano-laminated thin film metallic glass design for outstanding mechanical properties, *Scr. Mater.* 155 (2018) 73–77, <https://doi.org/10.1016/j.scriptamat.2018.06.015>.
- [50] M.D. Demetriou, M.E. Launey, G. Garrett, J.P. Schramm, D.C. Hofmann, W.L. Johnson, et al., A damage-tolerant glass, *Nat. Mater.* 10 (2011) 123–128, <https://doi.org/10.1038/nmat2930>.

- [51] M.D. Demetriou, G. Kaltenboeck, J.-Y. Suh, G. Garrett, M. Floyd, C. Crewdson, et al., Glassy steel optimized for glass-forming ability and toughness, *Appl. Phys. Lett.* 95 (2009), 41907, <https://doi.org/10.1063/1.3184792>.
- [52] A. Kawashima, H. Kurishita, H. Kimura, T. Zhang, A. Inoue, Fracture toughness of Zr55Al10Ni5Cu30 bulk metallic glass by 3-point bend testing, *Mater. Trans. JIM* 46 (2005) 1725–1732.
- [53] X.J. Gu, S.J. Poon, G.J. Shiflet, J.J. Lewandowski, Compressive plasticity and toughness of a Ti-based bulk metallic glass, *Acta Mater.* 58 (2010) 1708–1720, <https://doi.org/10.1016/j.actamat.2009.11.013>.
- [54] C.J. Gilbert, R.O. Ritchie, W.L. Johnson, Fracture toughness and fatigue-crack propagation in a Zr–Ti–Ni–Cu–Be bulk metallic glass, *Appl. Phys. Lett.* 71 (1997) 476–478, <https://doi.org/10.1063/1.119610>.
- [55] D.W. Smith, The antibonding effect, *J. Chem. Educ.* 77 (2000) 780, <https://doi.org/10.1021/ed077p780>.
- [56] A.S. Argon, Plastic deformation in metallic glasses, *Acta Metall.* 27 (1979) 47–58, [https://doi.org/10.1016/0001-6160\(79\)90055-5](https://doi.org/10.1016/0001-6160(79)90055-5).
- [57] S. Evertz, D. Music, V. Schnabel, J. Bednarcik, J.M. Schneider, Thermal expansion of Pd-based metallic glasses by ab initio methods and high energy X-ray diffraction, *Sci. Rep.* 7 (2017), 15744, <https://doi.org/10.1038/s41598-017-16117-7>.
- [58] D. Geissler, J. Freudenberger, H. Wendrock, M. Zimmermann, A. Gebert, On sample size effects in fracture toughness determination of bulk metallic glasses, *Eng. Fract. Mech.* 202 (2018) 500–507, <https://doi.org/10.1016/j.engfracmech.2018.09.020>.